Acta Pharmacologica Sinica

www.nature.com/aps

ARTICLE

Mitochondrial aldehyde dehydrogenase (ALDH2) rescues cardiac contractile dysfunction in an APP/PS1 murine model of Alzheimer's disease via inhibition of ACSL4-dependent ferroptosis

Zhi-yun Zhu[1], Yan-dong Liu[2], Yan Gong[2], Wei Jin[2], Elena Topchiy[3], Subat Turdi[3], Yue-feng Gao[3,4], Bruce Culver[3], Shu-yi Wang[3], Wei Ge[5], Wen-liang Zha[6,7], Jun Ren[3,8], Zhao-hui Pei[2] and Xing Qin[3,9]

Alzheimer's disease (AD) is associated with high incidence of cardiovascular events but the mechanism remains elusive. Our previous study reveals a tight correlation between cardiac dysfunction and low mitochondrial aldehyde dehydrogenase (ALDH2) activity in elderly AD patients. In the present study we investigated the effect of ALDH2 overexpression on cardiac function in APP/PS1 mouse model of AD. Global ALDH2 transgenic mice were crossed with APP/PS1 mutant mice to generate the ALDH2-APP/PS1 mutant mice. Cognitive function, cardiac contractile, and morphological properties were assessed. We showed that APP/PS1 mice displayed significant cognitive deficit in Morris water maze test, myocardial ultrastructural, geometric (cardiac atrophy, interstitial fibrosis) and functional (reduced fractional shortening and cardiomyocyte contraction) anomalies along with oxidative stress, apoptosis, and inflammation in myocardium. ALDH2 transgene significantly attenuated or mitigated these anomalies. We also noted the markedly elevated levels of lipid peroxidation, the essential lipid peroxidation enzyme acyl-CoA synthetase long-chain family member 4 (ACSL4), the transcriptional regulator for ACLS4 special protein 1 (SP1) and ferroptosis, evidenced by elevated NCOA4, decreased GPx4, and SLC7A11 in myocardium of APP/PS1 mutant mice; these effects were nullified by ALDH2 transgene. In cardiomyocytes isolated from WT mice and in H9C2 myoblasts in vitro, application of Aβ (20 μM) decreased cell survival, compromised cardiomyocyte contractile function, and induced lipid peroxidation; ALDH2 transgene or activator Alda-1 rescued Aβ-induced deteriorating effects. ALDH2-induced protection against Aβ-induced lipid peroxidation was mimicked by the SP1 inhibitor tolfenamic acid (TA) or the ACSL4 inhibitor triacsin C (TC), and mitigated by the lipid peroxidation inducer 5-hydroxyeicosatetraenoic acid (5-HETE) or the ferroptosis inducer erastin. These results demonstrate an essential role for ALDH2 in AD-induced cardiac anomalies through regulation of lipid peroxidation and ferroptosis.

Keywords: Alzheimer's disease; cardiac function; landscape perceptions; ALDH2; lipid peroxidation; ferroptosis; Alda-1; tolfenamic acid; triacsin C; 5-HETE; erastin

Acta Pharmacologica Sinica (2022) 43:39–49; https://doi.org/10.1038/s41401-021-00635-2

INTRODUCTION

Alzheimer's disease (AD), a neurodegenerative cognitive disease manifested by the buildup of amyloid β-peptide (Aβ) and neurofibrillary tangles (NFTs), is characterized by a progressive decline in memory and cognitive function and afflicts nearly 40 million individuals globally [1, 2]. The incidence of AD increases abruptly from 0.5% at 65 years of age to 8% after 85 years of age, which imposes heavy socioeconomic burdens related to health care [1–5]. Major brain changes develop throughout the course of AD, including atrophy, Aβ deposition, hyperphosphorylated tau protein leading to the formation of NFTs, neuronal death and inflammation [1, 2]. Ample evidence has revealed a close association between cardiovascular anomalies and AD onset [6–10]. In particular, AD patients often exhibit cardiac insufficiency, arrhythmia, and amyloid deposition in the heart [8, 9, 11–13]. The use of cardiac biomarkers has been endorsed in the clinical management of AD [14]. Among the reported etiological factors of AD, mutations in the β-amyloid precursor protein (APP), presenilin 1 (PS1), or presenilin 2 (PS2) are perceived to evoke the development of familial AD [15]. Earlier findings from our lab

[1]Jiangxi Provincial People's Hospital Affiliated to Nanchang University, Nanchang 330006, China; [2]The Second Department of Cardiology, The Third Hospital of Nanchang, Nanchang 330009, China; [3]University of Wyoming College of Health Sciences, Laramie, WY, USA; [4]State Key Laboratory of Animal Nutrition, College of Animal Science and Technology, China Agricultural University, Beijing 100083, China; [5]Department of General Practice, Xijing Hospital, the Air Force Military Medical University, Xi'an 710032, China; [6]Department of Surgery, Clinic Medical College, Hubei University of Science and Technology, Xianning 437100, China; [7]National Demonstration Center for Experimental General Medicine Education, Hubei University of Science and Technology, Xianning 437100, China; [8]Department of Cardiology and Shanghai Institute of Cardiovascular Diseases, Zhongshan Hospital Fudan University, Shanghai 200032, China and [9]Department of Cardiology, Xijing Hospital, the Air Force Military Medical University, Xi'an 710032, China
Correspondence: Jun Ren (jren_aldh2@outlook.com) or Zhao-hui Pei (peizhaohui@email.ncu.edu.cn) or Xing Qin (bravoqx@126.com)
These authors contributed equally: Zhi-yun Zhu, Yan-dong Liu, Yan Gong and Wei Jin

Received: 7 December 2020 Accepted: 26 February 2021
Published online: 25 March 2021

and others noted an essential role of PS1/PS2 in the regulation of cardiovascular function, including cardiac geometry, contractile capacity, and anatomical integrity (e.g., septal defects and double outlet right ventricles) [13, 16, 17]. In particular, Aβ deposition can be observed by as early as 4–6 months of age with full-blown amyloid β-peptide deposition occurring by 9 months of age in mice with overexpression of familial AD (FAD)-linked amyloid precursor protein with Swedish mutation and PS-1 with deletion of exon 9 ($APP^{swe}/PS1^{dE9}$) [18]. These APP/PS1 mice express a chimeric mouse/human amyloid precursor protein (Mo/HuAPP695swe) and a mutant human presenilin 1 (PS1-dE9) in central nervous system neurons and are widely used to study neurological disorders, particularly those associated with AD, amyloid plaque formation, and advanced aging [19]. Although a number of theories have been proposed for AD-evoked cardiovascular anomalies, including Aβ cytotoxicity, oxidative stress, abnormal protein aggregation, inflammation, excitotoxicity, and mitochondrial injury [8, 9, 13], the precise mechanism of AD-induced myocardial pathology remains poorly understood. Earlier findings revealed a vital role of gene polymorphisms in mitochondrial aldehyde dehydrogenase (ALDH2) in the development of neurodegenerative diseases, including AD [20–24]. For example, the age of AD onset was much younger in populations deficient in ALDH2 [25], although contrary findings were also encountered that seem to disprove the connection between ALDH2 polymorphisms and AD onset [26–28]. More recent evidence from our lab has shown a tight correlation between cardiac dysfunction and low ALDH2 activity in elderly (>80 years of age) AD patients [13], although little is known about the mechanism linking ALDH2 levels and AD-related cardiac anomalies.

Recent findings have demonstrated the contribution of ferroptosis, a form of regulated cell death characterized by the buildup of iron-based lipid reactive oxygen species (ROS), to the etiology of AD [29]. Ferroptosis participates in multiple organic pathologies, including liver, brain, heart, kidney, and intestinal diseases [29, 30]. Regulation of ferroptosis encompasses cystine/glutamate system Xc-mediated import of cystine, depletion of glutathione (GSH), and inhibition of glutathione peroxidase 4 (GPX4) [30]. Ferroptosis is implicated in pathological cell death in various forms of cerebrovascular diseases, including stroke, intracerebral hemorrhage, ischemia-reperfusion injury, heart failure, and cold stress [31, 32]. Moreover, autophagy, a conserved cellular process that governs cellular homeostasis under stress conditions [33], targets ferritin to autophagosomes through the autophagic cargo receptor nuclear receptor coactivator 4 (NCOA4) for lysosomal degradation of ferritin and evokes ferroptosis [30]. Unsurprisingly, triggering or inhibiting ferroptosis has been considered a novel therapeutic strategy for various human diseases [34]. In this context, the present study was designed to examine the role of ALDH2 overexpression in APP/PS1 mutation-induced cardiac contractile function and the mechanism involved with a special focus on lipid peroxidation and ferroptosis.

MATERIALS AND METHODS

Murine model of Alzheimer's disease and ALDH2 transgenic mice

All animal procedures used in this study were approved by the Animal Care and Use Committees at Nanchang University (Nanchang, China) and the University of Wyoming (Laramie, WY, USA) and were in compliance with the NIH standards. Briefly, 10-month-old male $APP^{swe}/PS1^{dE9}$ (APP/PS1) mutant mice were employed as an Alzheimer's disease model. The production of ALDH2 transgenic mice using the chicken β-actin promoter was described in detail previously [35, 36]. APP/PS1 mutant mice were crossed with ALDH2 transgenic mice (both on the C57BL/6 background) to generate heterozygotes that were further crossed to generate ALDH2-APP/PS1 mutant mice. The following four mouse groups were used in the study: the WT group (11 mice), the APP/PS1 group (10 mice), the ALDH2 group (11 mice), and the ALDH2-APP/PS1 group (11 mice).

Morris water maze test

The Morris water maze test was performed using a 120-cm (diameter) tank with distal visual cues filled with opaque water (25 °C). Mice were initially challenged to locate a colored platform (15 cm × 15 cm) from different quadrants in the pool. Each mouse underwent two trials daily for 8 days to locate the submerged platform. Following visible platform training, two consecutive days of hidden platform training were executed during which the platform was submerged in opaque water 1 cm deep (2 trials daily). Then, a probe trial was repeated in the absence of the platform. The latency to identify the platform and the less time spent in the target quadrant were measured using a computer-based video tracking system [13].

Echocardiographic assessment

Cardiac geometry and function were monitored in anesthetized (80 mg/kg ketamine and 12 mg/kg xylazine, i.p.) mice using a 2-D guided M-mode echocardiography (Vevo 2100, FUJIFILM Visualsonics, Toronto, ON, Canada) equipped with a 22–55 MHz linear transducer (MS550D, FUJIFILM VisualSonics). Left ventricular (LV) dimensions were recorded, and fractional shortening was calculated from LV end-diastolic (EDD) and end-systolic diameters (ESD) using the following equation: fractional shortening = (LVEDD − LVESD)/LVEDD. Ejection fraction, heart rate, and LV mass were derived as previously described [37].

Isolation of cardiomyocytes and in vitro drug treatment

Following ketamine/xylazine sedation, hearts were removed and perfused with Krebs-Henseleit bicarbonate (KHB) buffer containing the following components (in mM): 118 NaCl, 4.7 KCl, 1.2 $MgSO_4$, 1.2 KH_2PO_4, 25 $NaHCO_3$, 10 HEPES, and 11.1 glucose. The hearts were digested with collagenase D for 20 min. The left ventricles were removed and minced. The cardiomyocyte yield was ~75% and was not affected by APP/PS1 mutation or ALDH2 overexpression. Only rod-shaped myocytes with clear edges were selected for mechanical study [37, 38]. To determine the possible roles of the lipid peroxidation signals special protein 1 (SP1) and long-chain acyl-CoA synthetase-4 (ACSL4), lipid peroxidation and ferroptosis in APP/PS1 mutation-induced cardiomyocyte mechanical responses, cardiomyocytes were challenged with Aβ (20 μM) [10, 39] in the absence or presence of the SP1 inhibitor tolfenamic acid (TA, 30 μM) [40], the ACSL4 inhibitor triacsin C (TC, 10 μM) [41], the ferroptosis inducer erastin (20 μM) [42], or the lipid peroxidation inducer 5-hydroxyeicosatetraenoic acid (5-HETE, 50 μM) [43] prior to mechanical evaluation.

Cell shortening and relengthening

The mechanical properties of cardiomyocytes were assessed using an IonOptix™ soft-edge system (IonOptix, Milton, MA, USA). Cardiomyocytes were placed in a chamber mounted on the stage of an Olympus IX-70 microscope (Olympus Inc., Tokyo, Japan) and superfused (~2 mL/min at 25 °C) with KHB buffer containing 1 M $CaCl_2$. The myocytes were field stimulated at 0.5 Hz. Cell shortening and relengthening were assessed, including peak shortening (PS), time-to-PS (TPS), time-to-90% relengthening (TR_{90}), and maximal velocity of shortening/relengthening ($\pm dL/dt$) [44, 45].

Measurement of intracellular Ca^{2+}

A cohort of myocytes was loaded with Fura-2/AM (0.5 μM) for 15 min, and fluorescence intensity was recorded with a dual-excitation fluorescence photomultiplier system (Ionoptix). Fluorescence emissions were detected between 480 and 520 nm; qualitative change in Fura-2 fluorescence intensity (FFI) was

inferred from the Fura-2 fluorescence intensity ratio at the two wavelengths (360/380). Fluorescence decay time (single exponential) was calculated as an indicator of intracellular Ca^{2+} clearance. The cells were exposed to light emitted by a 75-W lamp while being stimulated to contract at a frequency of 0.5 Hz [44, 45].

ALDH2 activity
ALDH2 activity was measured in 33 mM sodium pyrophosphate containing 0.8 mM NAD^+, 15 μM propionaldehyde, and 0.1 mL protein extract. Propionaldehyde, the substrate of ALDH2, was oxidized in propionic acid, while NAD^+ was reduced to NADH to estimate ALDH2 activity. NADH was determined by measuring the spectrophotometric absorbance at 340 nm. ALDH2 activity is expressed as nmol NADH/min per mg protein [13].

Protein carbonyl assay
Proteins were extracted and minced to reduce proteolytic degradation. Protein was extracted using 20% trichloric acetic acid (TCA), and the samples were resuspended in a 10 mM 2,4-dinitrophenylhydrazine (2,4-DNPH) solution. Following centrifugation, the supernatants were removed, and the pellets were rinsed in ethanol:ethyl acetate and precipitated in 6 M guanidine solution. Absorbance was measured at 360–390 nm, and carbonyl content was determined using the molar absorption coefficient of 22,000 $M^{-1}{\cdot}cm^{-1}$ [46].

Analysis of reactive oxygen species (ROS)
The production of cellular ROS was evaluated by analyzing changes in fluorescence intensity resulting from oxidation of the intracellular fluoroprobe 5-(6)-chloromethyl-2′,7′-dichlorodihydrofluorescein diacetate (CM-H_2DCFDA, Molecular Probes, Eugene, OR, USA). Cardiomyocytes were loaded with the nonfluorescent dye H_2DCFDA (1 μM) at 37 °C for 30 min. Fluorescence intensity was measured using a fluorescence microplate reader at an excitation wavelength of 480 nm and an emission wavelength of 530 nm (Molecular Devices, Sunnyvale, CA, USA) [47].

Histological examination
After euthanasia, hearts were removed and placed in 10% neutral-buffered formalin for 24 h prior to fixation in paraffin. Five-micrometer myocardial sections were stained with fluorescein isothiocyanate (FITC)-conjugated wheat germ agglutinin. Cardiomyocyte cross-sectional areas were calculated on a digital microscope (×400) using ImageJ (version 1.34 S) software. Masson's trichrome staining was employed to estimate interstitial fibrosis. The percentage of fibrosis is shown as the fraction of the light blue-stained area normalized to the total area [32].

Transmission electron microscopy (TEM)
Small cubic pieces of left ventricles ≤1 mm^3 were fixed with 2.5% glutaraldehyde in 0.1 M sodium phosphate (pH 7.4) overnight at 4 °C prior to Epon Araldite embedding. Ultrathin sections (50 nm) were sliced using an ultramicrotome (Ultracut E, Leica) and stained with uranyl acetate and lead citrate. The specimens were imaged with a Hitachi H-7000 Electron Microscope (Pleasanton, CA, USA) equipped with a Gatan high-resolution digital camera [13].

Mitochondrial membrane potential measurement
Mitochondrial function was evaluated by detecting mitochondrial membrane potential. Briefly, cells were incubated with the MitoProbe™ JC-1 (tetraethylbenzimidazolylcarbocyanine iodide) assay kit (Thermo Fisher Scientific, Inc.) for 30 min at 37 °C. The nuclei were stained with 4,6-diamidino-2-phenylindole (DAPI) for 3 min at room temperature, and the mitochondrial potential was assessed under an Olympus IX81 inverted microscope (magnification, ×200) using FV10-ASW 1.7 software (both from Olympus Corporation, Tokyo, Japan). The red/green fluorescence intensities were separately recorded as grayscale intensities. The mitochondrial potential was quantified by evaluating the ratio of red-to-green fluorescence intensity [13].

Determination of mitochondrial permeability transition pore (mPTP) opening
mPTP opening was evaluated using NAD^+, a marker of mPTP opening. Briefly, cardiomyocytes were mixed thoroughly with perchloric acid (0.6 M). The mixture was homogenized, neutralized with potassium hydroxide (3 M), and centrifuged. The NAD^+ levels were determined fluorometrically using alcohol dehydrogenase with an excitation wavelength of 339 nm and emission wavelength of 460 nm [48].

Lipid peroxidation
A colorimetric assay (LPO-586 Kit; Oxis International, Portland, OR, USA) was used to determine the levels of malondialdehyde (MDA). Briefly, tissue homogenate was prepared using 20 mM Tris buffer containing 5 mM butylated hydroxytoluene (BHT) to prevent oxidation. The samples were incubated at 45 °C for 45 min followed by centrifugation for 10 min at 15,000 × *g* before the absorbance of supernatants was measured at 586 nm. Levels of analytes were determined using the molar extinction coefficient at 586 nm of 110,000 [32, 49]. For H9C2 cells, a lipid peroxidation assay kit (A106, Jiancheng, Nanjing, China) was used to evaluate lipid peroxidase; in this assay, lipid peroxide reacts with chromogenic reagents at 45 °C for 60 min to yield chromophores with a maximum absorption peak at 586 nm. Lipid ROS was measured using BODIPY 581/591 C11 (D3861, Invitrogen). Fluorescence was monitored using an Olympus fluorescence microscope [50].

MTT assay
The 3-(4,5-dimethylthiazol-2-yl)-2,5-diphenyltetrazolium bromide (MTT) assay is derived from transformation of the tetrazolium salt MTT to an insoluble formazan salt. Briefly, cardiomyocytes were plated in microtiter plates at a density of 3×10^5 cells/mL. MTT was added at a final concentration of 0.5 mg/mL, and plates were incubated for 2 h at 37 °C. Formazan crystals were dissolved in dimethyl sulfoxide (150 μL/well) and quantified spectroscopically at 560 nm using a SpectraMax® 190 spectrophotometer [48].

Western blot analysis
Samples (25 μg protein per lane) were separated on 10% SDS-polyacrylamide gels in a minigel apparatus (Mini-PROTEAN II, Bio-Rad) and transferred to nitrocellulose membranes prior to blocking with 5% milk in TBS-T. The membranes were incubated overnight at 4 °C with the following antibodies: anti-ALDH2, anti-Aβ, anti-PGC1α, anti-uncoupling protein 2 (UCP2), anti-interleukin-6 (IL-6), anti-tumor necrosis factor α (TNFα), anti-Bcl-2, anti-Bax, anti-SP1, anti-ACSL4, anti-solute carrier family 7 member 11 (SLC7A11, a ferroptosis marker), anti-GPx4, and anti-NCOA4 (a ferritin degradation autophagic cargo receptor). After immunoblotting, the films were scanned, and the immunoblot bands were detected using a Bio-Rad Calibrated Densitometer. GAPDH or α-tubulin was used as the loading control [13, 51].

Statistical analysis
Data are shown as the mean ± SEM. Statistical significance ($P < 0.05$) for each variable was estimated by analysis of variance (ANOVA) followed by Tukey's post hoc analysis.

RESULTS

Levels of ALDH2 expression and activity as well as the effect of the ALDH2 transgene on APP/PS1 mutation-induced cognitive function and biometric changes
ALDH2 protein expression and enzyme activity were examined in 2-, 5-, and 10-month-old WT and APP/PS1 mice. While neither

age nor the APP/PS1 mutation affected ALDH2 expression, the APP/PS1 mutation but not increased age overtly reduced ALDH2 activity at 5 and 10 months of age ($P = 0.0004$, Fig. 1a, b). The Morris water maze test revealed profound cognitive deficits in APP/PS1 mice manifested by increased escape latency and time spent in the target quadrant (TTQ) ($P < 0.001$). Although the ALDH2 transgene itself did not display any effect on cognitive function, it eliminated the APP/PS1 mutation-induced cognitive defects ($P < 0.001$, Fig. 1c, d). Neither the APP/PS1 mutation nor the ALDH2 transgene overtly affected body or organ (heart, liver, and kidney) weight, although the APP/PS1 mutation displayed a trend of cardiac atrophic remodeling ($P = 0.1594$), the effect of which was not discernable in ALDH2-APP/PS1 mice, and little effect was observed from the ALDH2 transgene alone (Fig. 1e–i). This result is in line with the significantly decreased cardiomyocyte cross-sectional area ($P = 0.0018$) and obvious interstitial fibrosis ($P < 0.0001$) in APP/PS1 mutant murine hearts, the effects of which were nullified by the ALDH2 transgene, whereas little effect was observed from the transgene alone (Fig. 1j–l).

Effect of the ALDH2 transgene on APP/PS1 mutation-induced changes in echocardiographic properties

Neither the APP/PS1 mutation nor the ALDH2 transgene nor the combination of both elicited any notable changes in LV wall thickness, septal wall thickness, LV end diastolic diameter (LV EDD), normalized LV mass, or heart rate ($P > 0.05$). Interestingly, the APP/PS1 mutation overtly increased LV end systolic diameter (LVESD) and decreased fractional shortening, ejection fraction and LV mass ($P < 0.0001$), and these effects were ablated by the ALDH2 transgene, whereas little effect was observed from the transgene alone (Fig. 2).

Effect of the ALDH2 transgene on APP/PS1 mutation-induced changes in cardiomyocyte mechanical and intracellular Ca^{2+} properties

To assess the potential mechanisms involved in the ALDH2-induced myocardial benefits, cardiomyocyte mechanical properties and intracellular Ca^{2+} handling were evaluated. Our data revealed that the APP/PS1 mutation impaired cardiomyocyte contractile and intracellular Ca^{2+} properties, as evidenced by decreased peak shortening (PS) and maximal velocity of shortening and relengthening ($\pm dL/dt$) as well as the electrically stimulated rise in intracellular Ca^{2+} (ΔFFI) ($P < 0.0003$), but did not affect the time-to-PS (TPS), time-to-90% relengthening (TR_{90}), resting intracellular Ca^{2+} level, or intracellular Ca^{2+} decay rate ($P > 0.05$). Consistent with its effect on echocardiographic function, ALDH2 negated APP/PS1 mutation-induced cardiomyocyte contractile, and intracellular Ca^{2+} defects without eliciting any effect by itself (Fig. 3).

Effect of the ALDH2 transgene on APP/PS1 mutation-induced changes in mitochondrial integrity and ROS production

The APP/PS1 mutation provoked a pronounced drop in mitochondrial membrane potential (MMP), as evaluated using JC-1 staining ($P < 0.0001$), and this effect was ablated by the ALDH2 transgene, whereas little effect was observed from the transgene alone (Fig. 4a, b). TEM assessment revealed overtly disrupted myofilament alignment and mitochondrial ultrastructure, as evidenced by the higher mitochondrial area (i.e., mitochondrial swelling,

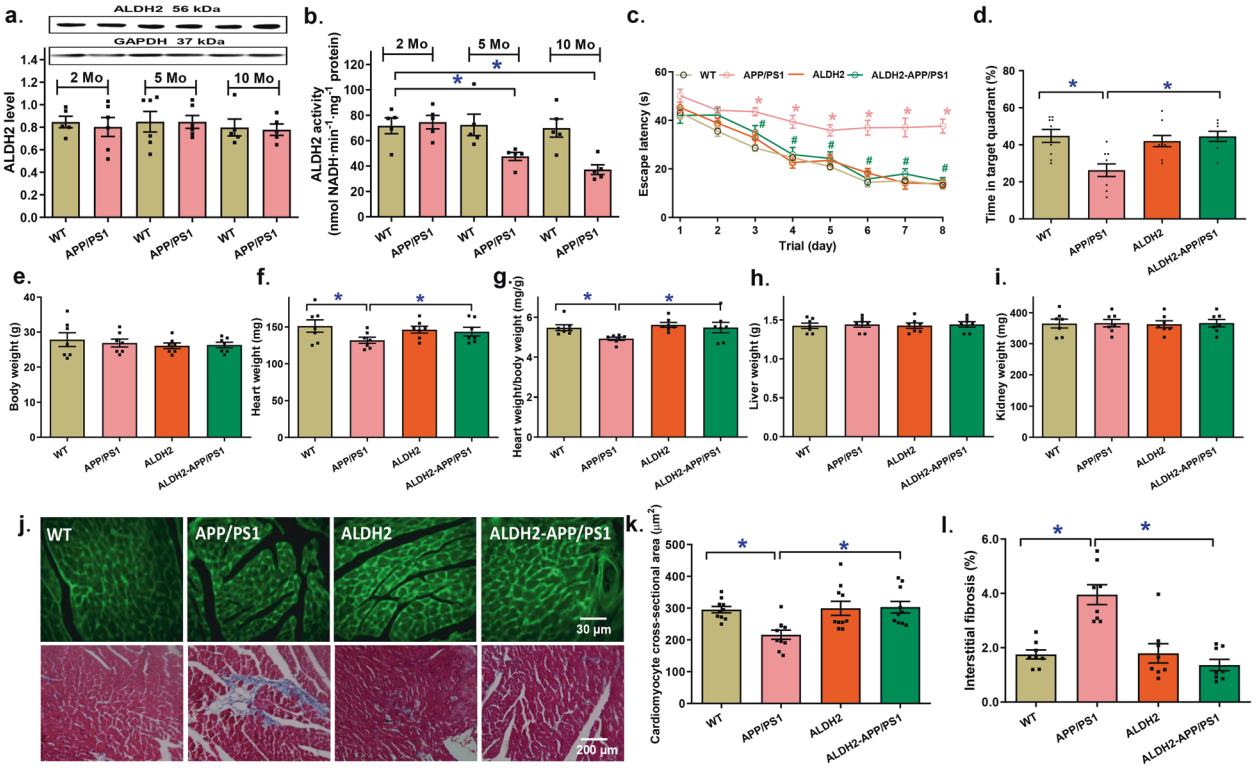

Fig. 1 The effect of age on myocardial ALDH2 expression and activity and the effect of ALDH2 overexpression on cognitive function, body and organ weight, and cardiac morphology in the APP/PS1 mouse model of Alzheimer's disease. a Myocardial ALDH2 levels at 2, 5, and 10 months of age; inset: representative gel bands depicting ALDH2 and GAPDH (loading control). **b** Myocardial ALDH2 activity at 2, 5, and 10 months of age; (**c**) Escape latency; (**d**) Time in target quadrant (%); (**e**) Body weight; (**f**) Heart weight; (**g**) Heart-to-body weight ratio; (**h**) Liver weight; (**i**) Kidney weight. **j** Representative images of FITC-lectin (×200) and Masson's trichrome staining (×100) showing myocardial morphology. **k** Quantitative analysis of FITC-lectin cardiomyocyte cross-sectional area. **l** Quantitative analysis of fibrotic area (Masson's trichrome-stained area in light blue color normalized to total cardiac area). Mean ± SEM, $n = 7–8$ mice per group, $^*P < 0.05$ between the indicated groups.

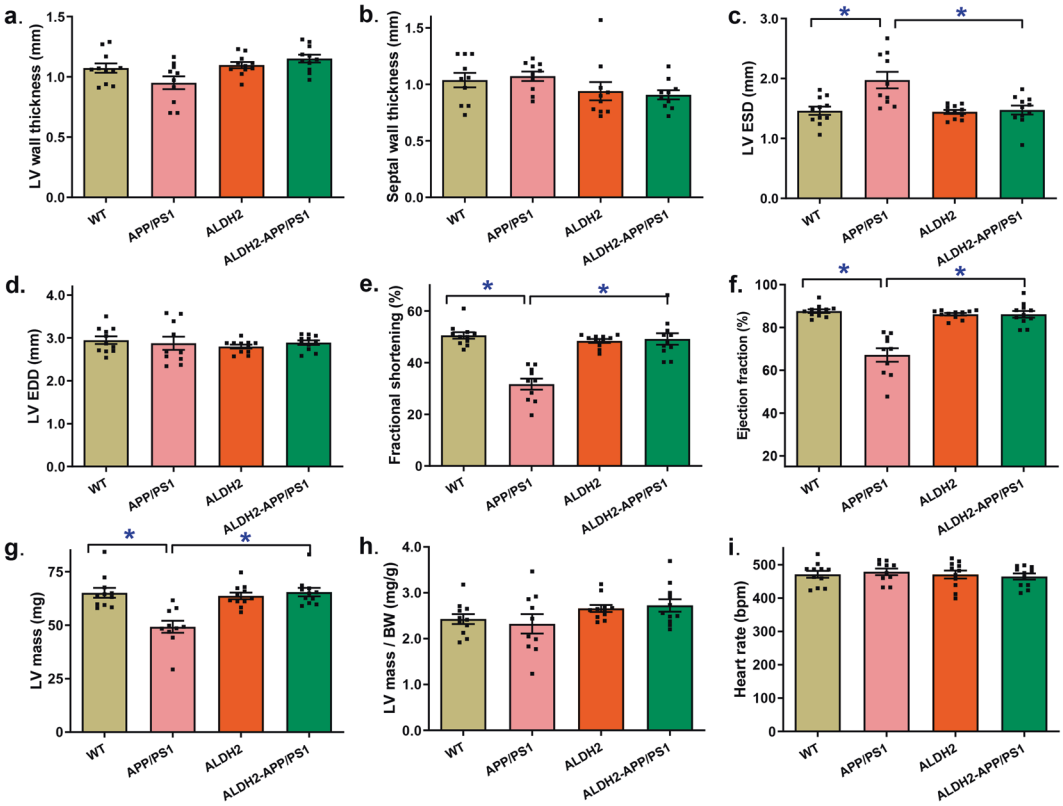

Fig. 2 Effect of ALDH2 overexpression on echocardiographic properties in the APP/PS1 mouse model of Alzheimer's disease. a Left ventricular (LV) wall thickness; (**b**) Septal wall thickness; (**c**) LV end systolic volume (LVESD); (**d**) LV end diastolic volume (LVEDD); (**e**) Fractional shortening; (**f**) Ejection fraction; (**g**) LV mass; (**h**) LV mass-to-body weight ratio; (**i**) Heart rate. Mean ± SEM, $n = 10–11$ mice per group, $^*P < 0.05$ between the indicated groups.

$P = 0.0002$) and decreased mitochondrial number (i.e., mitochondrial injury, $P < 0.0001$). Although the ALDH2 transgene itself failed to elicit any overt effect on myocardial ultrastructure, it nullified the APP/PS1 mutation-induced myocardial ultrastructural anomalies. This result was in line with the APP/PS1 mutation- and ALDH2-induced changes in ROS production ($P < 0.0001$, Fig. 4c–g). Assessment of mitochondrial damage using mPTP revealed decreased NAD^+ levels in APP/PS1 mice indicating mPTP opening; this effect was absent in ALDH2-APP/PS1 mice, and the ALDH2 transgene itself showed little effect ($P = 0.0003$, Fig. 4h). Moreover, the APP/PS1 mutation downregulated the mitochondrial biogenesis cofactor peroxisome proliferator-activated receptor-gamma coactivator 1α (PGC1α, $P = 0.0301$) and mitochondrial uncoupling protein 2 (UCP2, $P = 0.0305$), and these effects were reversed by the ALDH2 transgene, whereas little effect was observed from ALDH2 alone (Fig. 4i, j).

The effects of ALDH2 on APP/PS1 mutation-induced apoptosis, ferroptosis, and inflammation

We then assessed the levels of various cell death proteins and noted increases in Aβ deposition ($P = 0.0001$) and Bax expression ($P < 0.0001$) and downregulated Bcl-2 levels ($P < 0.0001$); these effects were eliminated by ALDH2. The levels of ALDH2 were validated in ALDH2 transgenic mice (Fig. 5a–c). To determine the possible involvement of inflammation and oxidative stress in APP/PS1 mutation- and ALDH2-induced changes in myocardial function, the levels of TNFα and IL-6 and the GSH-to-oxidized glutathione (GSSG) ratio were determined. Our data revealed pronounced elevation in the proinflammatory protein markers TNFα and IL-6 along with a decreased GSH-GSSG ratio (all with $P < 0.0002$) in hearts from APP/PS1 mice, and these effects were eliminated by the ALDH2 transgene, whereas little effect observed from the transgene alone (Fig. 5f–h).

Assessment of protein damage, lipid peroxidation and levels of essential regulators of lipid peroxidation, including carbonyl formation, MDA, SP1, and ACSL4, revealed significant increases ($P < 0.0001$) in protein damage, lipid peroxidation markers and related signaling molecules in hearts from APP/PS1 mice. Similarly, lipid peroxidation downstream of ferroptosis was also evident in APP/PS1 murine hearts, as shown by upregulated levels of the ferroptosis autophagy marker NCOA4 ($P = 0.0022$) and downregulated levels of GPx4 ($P = 0.004$) and SLC7A11 ($P = 0.002$). Although the ALDH2 transgene evoked little effect on lipid peroxidation and ferroptosis, it overtly nullified APP/PS1 mutation-induced lipid peroxidation and ferroptosis (Fig. 6). These data suggested possible roles of inflammation, lipid peroxidation, and ferroptosis in ALDH2-elicited cardioprotection in APP/PS1 mutant mice.

Role of lipid peroxidation and ferroptosis in the ALDH2-induced protective effects against Aβ-induced cell death, cardiomyocyte dysfunction and lipid peroxidation

To determine the cause-effect relationship of lipid peroxidation and ferroptosis in the ALDH2-induced cardioprotection observed in APP/PS1 mutant mice, adult cardiomyocytes from WT mice were challenged with Aβ (20 μM) [10, 39] for 8 h in the absence or presence of the SP1 inhibitor tolfenamic acid (TA) or the ACSL4 inhibitor triacsin C (TC). A cohort of cardiomyocytes from ALDH2 transgenic mice were incubated with Aβ (20 μM) in the presence or absence of the ferroptosis activator erastin or the lipid peroxidation inducer 5-HETE. As expected, incubation with Aβ overtly decreased cell survival, as shown by MTT assays, and compromised cardiomyocyte contractile function, as evidenced by

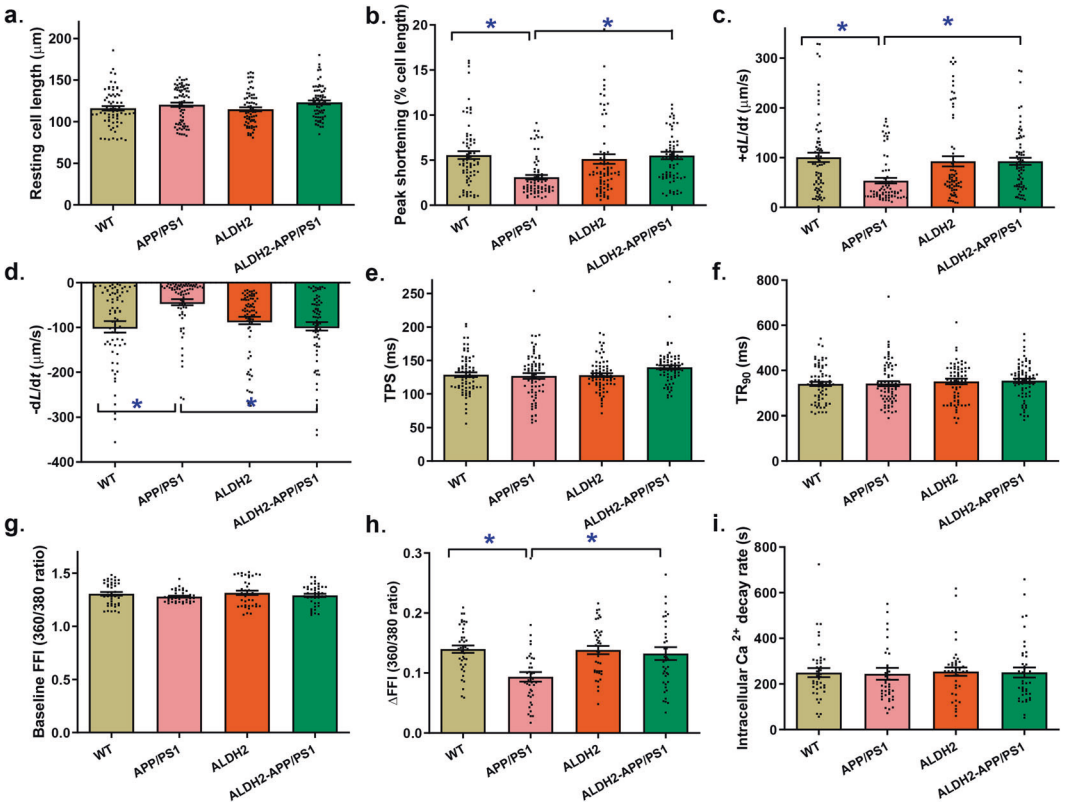

Fig. 3 Effect of ALDH2 overexpression on cardiomyocyte mechanical and intracellular Ca^{2+} properties in the APP/PS1 mouse model of Alzheimer's disease. a Resting cell length; (**b**) Peak shortening; (**c**) Maximal velocity of cell shortening (+d*L*/d*t*); (**d**) Maximal velocity of cell relengthening (−d*L*/d*t*); (**e**) Time-to-peak shortening (TPS); (**f**) Time-to-90% relengthening (TR_{90}); (**g**) Baseline Fura-2 fluorescence intensity (FFI); (**h**) Electrically stimulated rise in FFI (ΔFFI); (**i**) Intracellular Ca^{2+} decay rate. Mean ± SEM, $n = 71$ (panels **a**–**f**) or 40 (panels **g**–**i**) cells from 5–6 mice per group, $^*P < 0.05$ between the indicated groups.

decreased PS and ± d*L*/d*t* (all with $P < 0.0001$) in addition to unchanged resting cell length (data not shown), TPS, and TR_{90}; these effects were nullified by TA, TC, or ALDH2, whereas each intervention showed little effect alone. Interestingly, the ALDH2-induced beneficial effect was eliminated by erastin and 5-HETE, which showed little effect themselves (Fig. 7a–f). Further assessment of lipid peroxidation noted similar findings. Aβ incubation overtly evoked lipid peroxidation ($P < 0.0001$), and this effect was negated by TA, TC, or ALDH2, which showed minimal effects themselves. Similarly, the ALDH2-induced protection against Aβ-induced lipid peroxidation was mitigated by erastin and 5-HETE, which showed little effect themselves (Fig. 8a, b). These data indicated important roles of SP1 and ACSL4 signaling in Aβ-induced changes in cell survival, cardiomyocyte contractile dysfunction, and lipid peroxidation, while reducing ferroptosis and lipid peroxidation played a vital role in ALDH2-induced cardioprotection.

DISCUSSION

The salient findings from our study demonstrated decreased myocardial ALDH2 activity in APP/PS1 mice at 5 and 10 months of age and overt protective effects of the ALDH2 transgene against APP/PS1 mutation-induced cognitive deficits, cardiac remodeling and dysfunction, mitochondrial defects, apoptosis, protein damage, and inflammation. More interestingly, SP1-ACSL4-mediated regulation of lipid peroxidation and ferroptosis was involved in ALDH2-mediated cardioprotection in an APP/PS1 murine model of AD. These findings support the therapeutic potential of targeting ALDH2, lipid peroxidation, and ferroptosis in AD-induced cardiac anomalies.

Data from our study indicated cardiac remodeling (atrophy) and contractile dysfunction in the APP/PS1 model of AD that was reminiscent of observations made in humans [7] and experimental models of AD [17, 52, 53]. Our study noted loss of myocardial ALDH2 activity but not expression in APP/PS1 murine hearts, consistent with our earlier findings [13]. More importantly, a beneficial effect of ALDH2 in cognitive function in the APP/PS1 mutant mice was noted. In particular, ALDH2 rescued mitochondrial integrity and reduced mitochondrial damage (as evidenced by mPTP opening), apoptosis, protein damage and inflammation (as evidenced by TNFα and IL-6) in APP/PS1 mutant mice, which also showed restored mitochondrial membrane potential and levels of PGC1α and UCP2. To date, mixed findings have been reported regarding the role of ALDH2 in AD pathology. ALDH2 genetic polymorphism was reported to evoke an increased risk of AD [22, 23, 25], although conflicting data were also reported [26–28]. The findings from our current study favor the notion that ALDH2 helps to alleviate cognitive deficits and cardiac dysfunction in the APP/PS1 mutant murine model of AD. More intriguingly, our study noted roles of lipid peroxidation and ferroptosis in APP/PS1 mutation-induced cardiac defects. ALDH2 nullified AD-induced cardiac atrophic remodeling, contractile dysfunction, intracellular Ca^{2+}, apoptosis, proinflammation, protein damage, and mitochondrial defects accompanied by inhibition of lipid peroxidation and ferroptosis. Recent evidence from Chen and colleagues has revealed a novel lipid peroxidation-dependent mechanism by which ALDH2 regulates mitochondrial fission and vascular smooth muscle cell proliferation in pulmonary hypertension [54]. Interestingly, our in vitro evidence suggested that induction of lipid peroxidation and ferroptosis using 5-HETE and erastin, respectively, nullified the ALDH2- or Alda-1-induced protective effects

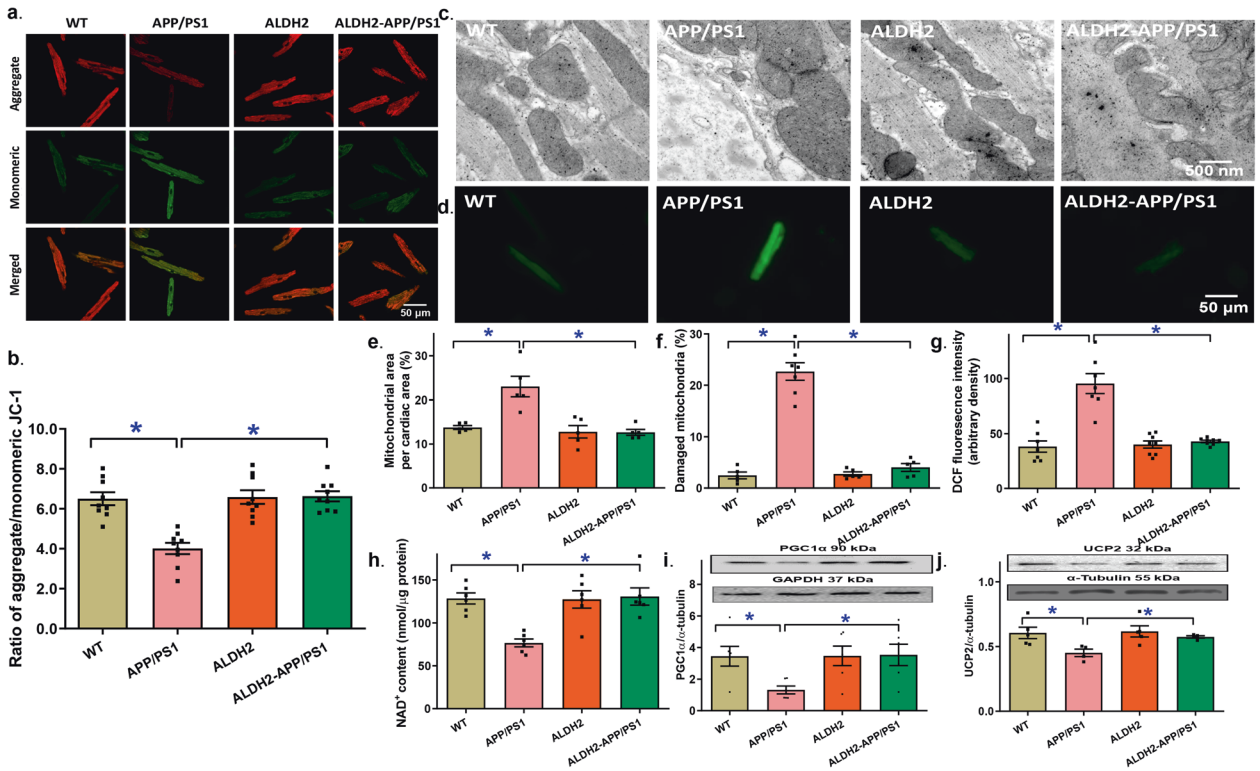

Fig. 4 Mitochondrial membrane potential, mitochondrial permeability transition pore (mPTP) opening, myocardial ultrastructure, and reactive oxygen species (ROS) production in hearts from the APP/PS1 mouse model of Alzheimer's disease with or without the ALDH2 transgene. a Representative images of JC-1 fluorescence in cardiomyocytes from various groups (**b**) Pooled data depicting the ratio of aggregate/monomeric JC-1; (**c**) Representative transmission electron microscopy (TEM) ultrastructural images (×15,000); (**d**) Representative DCF fluorescent images depicting ROS production; (**e**) Mitochondrial area per cardiac area; (**f**) Percentage of damaged mitochondria; (**g**) Pooled data from DCF staining depicting ROS levels; (**h**) mPTP opening evaluated using NAD^+ levels; (**i**) Levels of PGC1α; (**j**) Levels of UCP2. Insets: representative gel blots showing the levels of the mitochondrial proteins PGC1α and UCP2 using specific antibodies (α-tubulin was used as the loading control). Mean ± SEM, $n = 7–9$ images or mice per group ($n = 5–6$ images for panels **e**, **f**, and **h**). *$P < 0.05$ between the indicated groups.

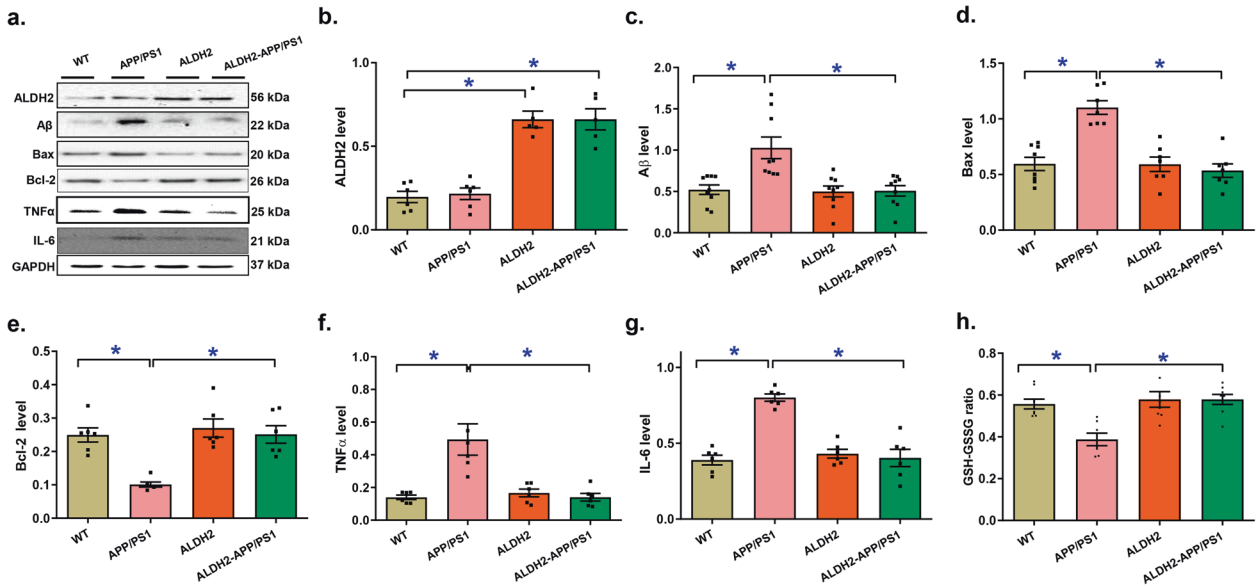

Fig. 5 Levels of ALDH2, Aβ, and markers of apoptosis and inflammation in the myocardium of the APP/PS1 mouse model of Alzheimer's disease with or without ALDH2 overexpression. a Representative gel bands depicting ALDH2, Aβ, and apoptosis and inflammation markers using specific antibodies (GAPDH was used as the loading control). **b** Levels of ALDH2; (**c**) Levels of Aβ; (**d**) Levels of Bax; (**e**) Levels of Bcl-2; (**f**) Levels of TNFα; (**g**) Levels of IL-6, and (**h**) GSH-GSSG ratio. Mean ± SEM, $n = 6–9$ mice per group, *$P < 0.05$ between the indicated groups.

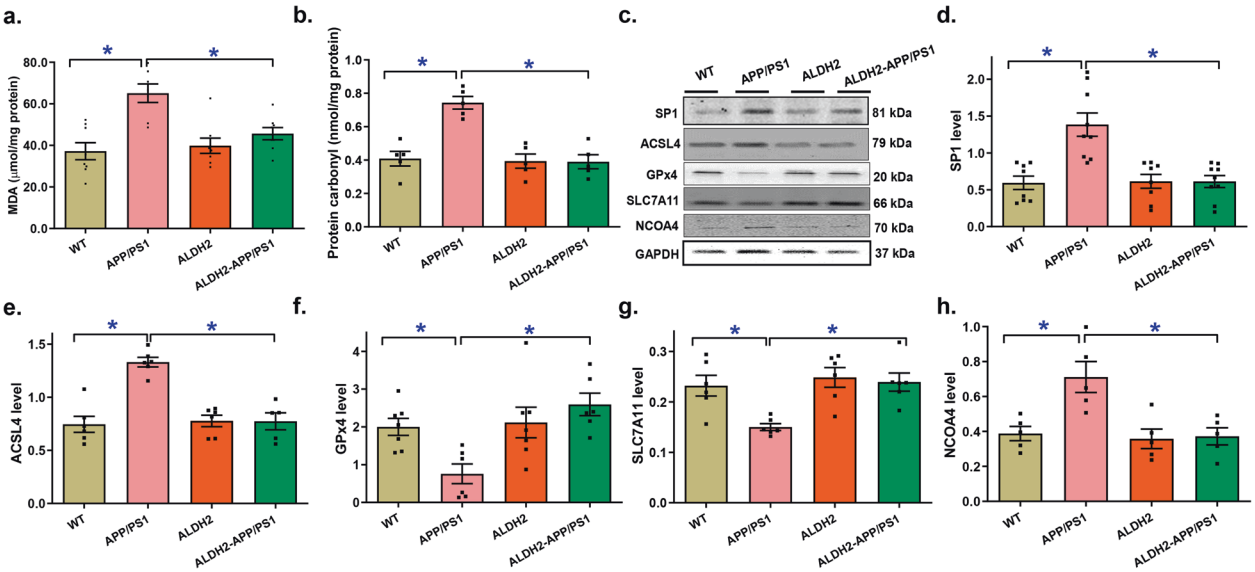

Fig. 6 Levels of protein carbonyl damage, lipid peroxidation, the lipid peroxidation regulatory signals SP1 and ACSL4, and ferroptosis in myocardium from the APP/PS1 mouse model of Alzheimer's disease with or without ALDH2 overexpression. **a** Levels of MDA; (**b**) Levels of protein carbonyl; (**c**) Representative gel bands depicting SP1, ACSL4, and ferroptosis protein markers using specific antibodies (GAPDH was used as the loading control); (**d**) Levels of SP1; (**e**) Levels of ACSL4; (**f**) Levels of GPx4; (**g**) Levels of SLC7A11; (**h**) Levels of NCOA4. Mean ± SEM, $n = 6–9$ mice per group, $^*P < 0.05$ between the indicated groups.

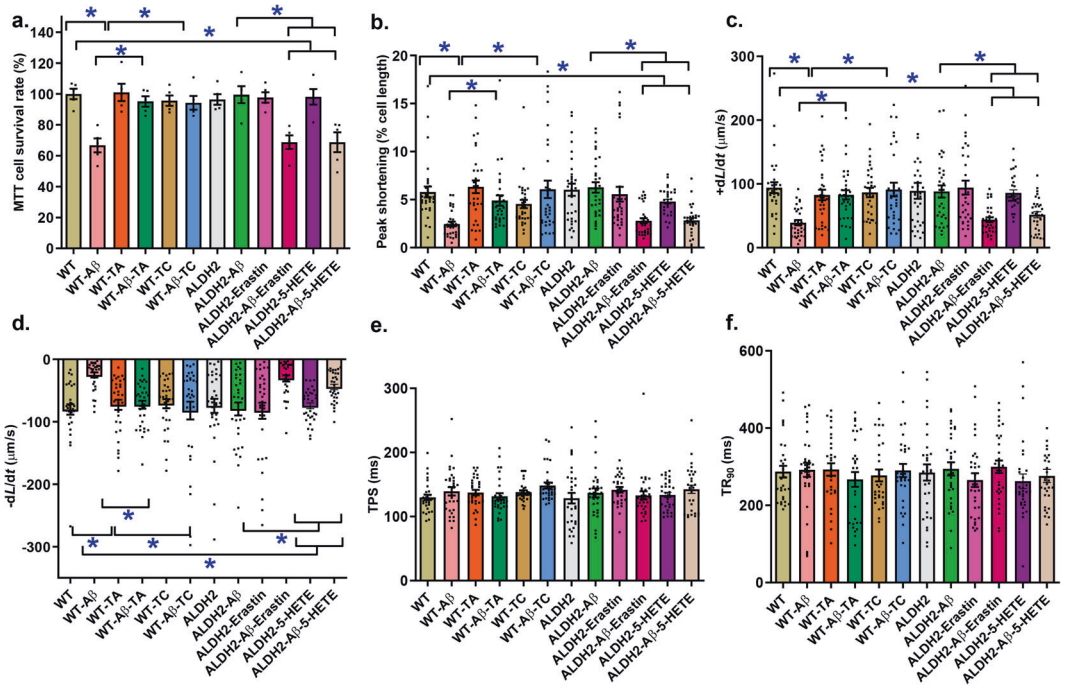

Fig. 7 Effects of Aβ challenge, inhibition of SP1 and ACSL4 or induction of lipid peroxidation and ferroptosis on cardiomyocyte survival and contractile responses in isolated cardiomyocytes from WT and ALDH2 transgenic mice. Cardiomyocytes from WT and ALDH2 transgenic mice were treated with Aβ (20 μM) for 6 h in the absence or presence of the SP1 inhibitor tolfenamic acid (TA, 50 μM), the ACSL4 inhibitor triacsin C (TC, 10 μM), the ferroptosis inducer erastin (20 μM) or the lipid peroxidation inducer 5-hydroxyeicosatetraenoic acid (5-HETE, 1 μM) prior to assessment of cardiomyocyte mechanical function. **a** Cell survival evaluated using MTT assay; (**b**) Peak shortening (normalized to cell length); (**c**) Maximal velocity of shortening (+d*L*/d*t*); (**d**) Maximal velocity of relengthening (-d*L*/d*t*); (**e**) Time-to-peak shortening (TPS); (**f**) Time-to-90% relengthening (TR_{90}). Mean ± SEM, $n = 5$ isolations (panel **a**) or 31 cells (panels **b**–**f**) per group, $^*P < 0.05$ between the indicated groups.

against Aβ-induced cell death, as shown by MTT assays, as well as cardiomyocyte dysfunction and lipid peroxidation. These findings collectively favor a possible obligatory role for lipid peroxidation and ferroptosis in APP/PS1 mutation- and ALDH2-evoked cardiac responses.

Recent evidence has suggested unique roles of ferroptosis in both neurodegenerative and cardiovascular diseases [5, 29, 31], although little is known about the role of ferroptosis in AD-associated cardiovascular dysfunction. Our results showed elevated ferroptosis in APP/PS1 mutant mouse hearts involving the

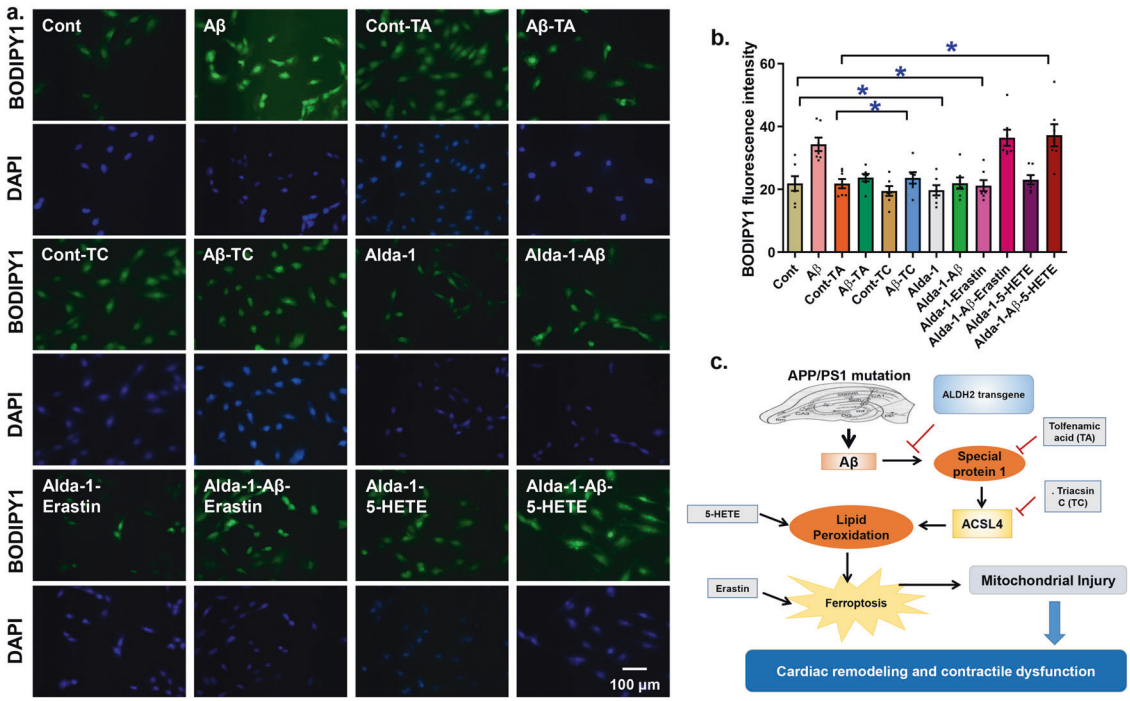

Fig. 8 Effect of Aβ challenge, ALDH2 activation, inhibition of SP1 and ACSL4 or induction of lipid peroxidation and ferroptosis on lipid peroxidation in H9C2 myoblasts. H9C2 cells were incubated with Aβ (20 μM) for 24 h in the absence or presence of the ALDH2 activator Alda-1 (20 μM), the SP1 inhibitor tolfenamic acid (TA, 50 μM), the ACSL4 inhibitor triacsin C (TC, 10 μM), the ferroptosis inducer erastin (20 μM) or the lipid peroxidation inducer 5-HETE (10 μM) prior to assessment of lipid peroxidation using BODIPY1 C11 imaging. **a** Representative image depicting cells from the various treatment groups; (**b**) Pooled BODIPY1 C11 fluorescence intensity data; and (**c**) Schematic diagram depicting our working model of the protective effects of ALDH2 against APP/PS1 mutation-associated pathological changes in cardiac remodeling and function. APP/PS1 mutation evokes the accumulation of Aβ and the induction of SP1-ACSL4-mediated lipid peroxidation and ferroptosis, ultimately evoking mitochondrial injury and cardiac damage. ALDH2 disrupts the Aβ-induced increase in SP1/ACSL4 to suppress lipid peroxidation and ferroptosis, thus preserving cardiac homeostasis under APP/PS1 mutation. Mean ± SEM, $n = 7$ independent cell cultures per group, $^*P < 0.05$ between the indicated groups.

upregulation of SP1 and ACSL4. ACSL4 is heavily involved in intracellular lipid storage, cholesterol transport from the endoplasmic reticulum (ER) into mitochondria, and the regulation of arachidonic acid and its metabolites [55]. Moreover, ACSL4 is an indispensable player in lipid peroxidation, which is necessary for ferroptosis [55]. SP1 is a classic transcription factor capable of turning on target genes by binding to GC box elements in promoter regions. The *ACSL4* gene contains many GC boxes and, unsurprisingly, was reported to be a unique target of SP1 [50]. Indeed, with inhibition of the upstream signaling molecule SP1, Aβ-induced cardiomyocyte cell death, and contractile dysfunction were mitigated, suggesting an indispensable role of SP1 and ACSL4 in APP/PS1 mutation-induced myopathic changes. ALDH2 plays an essential role in the maintenance of cardiovascular homeostasis in stress settings such as alcoholism, doxorubicin cardiomyopathy, ischemic disease, sepsis, stroke, and metabolic diseases [35, 36, 56–62]. In our hands, ALDH2 rescued APP/PS1 mutation-induced cardiac anomalies via inhibition of SP1-ACSL4-mediated lipid peroxidation and ferroptosis. Our current data further showed that ALDH2 countered APP/PS1 mutation-induced upregulation of SP1, ACSL4, lipid peroxidation, and ferroptosis, as evidenced by downregulation of the ferroptosis markers GPx4 and SLC7A11 and upregulation of the ferroptosis autophagy adaptor NCOA4. Given the nature of ALDH2 as an intrinsic mitochondrial protein that preserves mitochondrial integrity [54, 61], increases in ALDH2 levels or activity in the APP/PS1 model of AD should help to preserve mitochondrial integrity to alleviate lipid peroxidation.

Experimental limitations: although our findings suggested that ALDH2 was effective in reconciling APP/PS1 mutation-induced cardiac atrophy and contractile dysfunction, a number of issues remain to be resolved. First, ALDH2 genetic polymorphisms in human subjects display mixed effects on the risk of dementia and Alzheimer's disease; thus, compensatory machinery may exist to offset the loss of ALDH2 in individuals with ALDH2 mutations. Second, as pharmacological activators of ALDH2 (such as Alda-1) [59] are becoming increasingly recognized in experimental and preclinical settings, the toxicity of these ALDH2 activators remains a major obstacle to their clinical application. More intensive efforts are warranted to identify specific and less toxic ALDH2 regulators. Although pharmacological inhibitors of SP1, ACSL4, lipid peroxidation, and ferroptosis may be considered downstream executors of ALDH2, limited information is readily available on the pharmacodynamics, pharmacokinetics, specificity, and efficacy of these reagents. Further study is required to better illustrate the precise role of SP1-ACSL4-ferroptosis signaling in neurological function using genetically engineered animal models. Finally, although ALDH2 mitigated the APP/PS1-induced upregulation of myocardial inflammation (TNFα and IL-6) and apoptosis, the precise role of inflammation and apoptosis as well as other cell death-related pathways, such as necroptosis and autophagy, in ALDH2- and APP/PS1-induced changes in ferroptosis and mitochondrial injury remain uncertain.

In conclusion, the findings from our current work provide the first evidence that the ALDH2 transgene effectively protects against APP/PS1 mutation-induced cardiac atrophy, contractile dysfunction, and mitochondrial injury via SP1-ACSL4-mediated regulation of lipid peroxidation and ferroptosis (Fig. 8c). This conclusion is supported by the observation that inhibition of SP1 and ACSL4 mimicked the beneficial effects of ALDH2 overexpression in APP/PS1 mutant mice, while induction of lipid peroxidation and ferroptosis suppressed these effects. Although it

is premature to predict the precise therapeutic value of targeting ALDH2 and ferroptosis in Alzheimer's disease-induced myopathic anomalies, these findings should shed some light on the clinical utility of ALDH2 and ferroptosis in cardiovascular dysfunction in patients with neurodegenerative diseases.

ACKNOWLEDGEMENTS

The research reported in this publication was supported in part by the National Natural Science Foundation of China (82060351, 82000351) and the Natural Science Foundation of Jiangxi Province (20203BBGL73189).

AUTHOR CONTRIBUTIONS

ZYZ, YDL, YG, WJ, ET, ST, YFG, SYW, WLZ, and XQ performed the experiments; JR, BC, WG, ZHP, and XQ conceived and designed the study and drafted, edited, and approved the paper.

ADDITIONAL INFORMATION

Competing interests: The authors declare no competing interests.

REFERENCES

1. Jellinger KA. Pathobiological subtypes of Alzheimer disease. Dement Geriatr Cogn Disord. 2020;49:321–33.
2. Robinson M, Lee BY, Hanes FT. Recent progress in Alzheimer's disease research, part 2: genetics and epidemiology. J Alzheimers Dis. 2018;61:459.
3. Ryan KC, Ashkavand Z, Norman KR. The role of mitochondrial calcium homeostasis in Alzheimer's and related diseases. Int J Mol Sci. 2020;21:9153.
4. Zhang F, Zhong RJ, Cheng C, Li S, Le WD. New therapeutics beyond amyloid-beta and tau for the treatment of Alzheimer's disease. Acta Pharmacol Sin. 2021. in press. https://doi.org/10.1038/s41401-020-00565-5.
5. Johnson J, Mercado-Ayon E, Mercado-Ayon Y, Dong YN, Halawani S, Ngaba L, et al. Mitochondrial dysfunction in the development and progression of neurodegenerative diseases. Arch Biochem Biophys 2021. https://doi.org/10.1016/j.abb.2020.108698.
6. Troncone L, Luciani M, Coggins M, Wilker EH, Ho CY, Codispoti KE, et al. Abeta amyloid pathology affects the hearts of patients with Alzheimer's disease: mind the heart. J Am Coll Cardiol. 2016;68:2395–407.
7. Sanna GD, Nusdeo G, Piras MR, Forteleoni A, Murru MR, Saba PS, et al. Cardiac abnormalities in Alzheimer disease: clinical relevance beyond pathophysiological rationale and instrumental findings? JACC Heart Fail. 2019;7:121–8.
8. Tublin JM, Adelstein JM, Del Monte F, Combs CK, Wold LE. Getting to the heart of Alzheimer disease. Circ Res. 2019;124:142–9.
9. Yang M, Li C, Zhang Y, Ren J. Interrelationship between Alzheimer's disease and cardiac dysfunction: the brain-heart continuum? Acta Biochim Biophys Sin (Shanghai). 2020;52:1–8.
10. Zhang B, Bian X, He P, Fu X, Higuchi K, Yang X, et al. The toxicity mechanisms of action of Abeta25-35 in isolated rat cardiac myocytes. Molecules. 2014;19:12242–57.
11. Benenati S, Canale C, De Marzo V, Della Bona R, Rosa G, Porto I. Atrial fibrillation and Alzheimer disease: a conundrum. Eur J Clin Invest. 2021. https://doi.org/10.1111/eci.13451.
12. Omoya R, Miyajima M, Ohta K, Suzuki Y, Aoki A, Fujiwara M, et al. Heart rate response to orthostatic challenge in patients with dementia with Lewy bodies and Alzheimer's disease. Psychogeriatrics. 2021;21:62–70.
13. Wang S, Wang L, Qin X, Turdi S, Sun D, Culver B, et al. ALDH2 contributes to melatonin-induced protection against APP/PS1 mutation-prompted cardiac anomalies through cGAS-STING-TBK1-mediated regulation of mitophagy. Signal Transduct Target Ther. 2020;5:119.
14. Khan S, Kamal MA. Cardiac biomarkers in stroke, Alzheimer's disease, and other dementia. Are they of use? A brief overview of data from recent investigations. CNS Neurol Disord Drug Targets. 2021. https://doi.org/10.2174/1871527319666201005171003.
15. Mohmmad Abdul H, Wenk GL, Gramling M, Hauss-Wegrzyniak B, Butterfield DA. APP and PS-1 mutations induce brain oxidative stress independent of dietary cholesterol: implications for Alzheimer's disease. Neurosci Lett. 2004;368:148–50.
16. Nakajima M, Moriizumi E, Koseki H, Shirasawa T. Presenilin 1 is essential for cardiac morphogenesis. Dev Dyn. 2004;230:795–9.
17. Turdi S, Guo R, Huff AF, Wolf EM, Culver B, Ren J. Cardiomyocyte contractile dysfunction in the APPswe/PS1dE9 mouse model of Alzheimer's disease. PLoS One. 2009;4:e6033.
18. Taniuchi N, Niidome T, Goto Y, Akaike A, Kihara T, Sugimoto H. Decreased proliferation of hippocampal progenitor cells in APP^{swe}/PS1^{dE9} transgenic mice. Neuroreport. 2007;18:1801–5.
19. Webster SJ, Bachstetter AD, Nelson PT, Schmitt FA, Van Eldik LJ. Using mice to model Alzheimer's dementia: an overview of the clinical disease and the preclinical behavioral changes in 10 mouse models. Front Genet. 2014;5:88.
20. Chen CH, Sun L, Mochly-Rosen D. Mitochondrial aldehyde dehydrogenase and cardiac diseases. Cardiovasc Res. 2010;88:51–7.
21. Hao PP, Chen YG, Wang JL, Wang XL, Zhang Y. Meta-analysis of aldehyde dehydrogenase 2 gene polymorphism and Alzheimer's disease in East Asians. Can J Neurol Sci. 2011;38:500–6.
22. Ma L, Lu ZN. Role of ADH1B rs1229984 and ALDH2 rs671 gene polymorphisms in the development of Alzheimer's disease. Genet Mol Res. 2016;15, https://doi.org/10.4238/gmr.15048740.
23. Chen J, Huang W, Cheng CH, Zhou L, Jiang GB, Hu YY. Association between aldehyde dehydrogenase-2 polymorphisms and risk of Alzheimer's disease and Parkinson's disease: a meta-analysis based on 5,315 Individuals. Front Neurol. 2019;10:290.
24. Wang B, Wang J, Zhou S, Tan S, He X, Yang Z, et al. The association of mitochondrial aldehyde dehydrogenase gene (ALDH2) polymorphism with susceptibility to late-onset Alzheimer's disease in Chinese. J Neurol Sci. 2008;268:172–5.
25. Ohta S. [Roles of mitochondrial dysfunctions in Alzheimer's disease–contribution of deficiency of ALDH 2]. Rinsho Shinkeigaku. 2000;40:1231–3.
26. Komatsu M, Shibata N, Ohnuma T, Kuerban B, Tomson K, Toda A, et al. Polymorphisms in the aldehyde dehydrogenase 2 and dopamine beta hydroxylase genes are not associated with Alzheimer's disease. J Neural Transm (Vienna). 2014;121:427–32.
27. Shin IS, Stewart R, Kim JM, Kim SW, Yang SJ, Shin HY, et al. Mitochondrial aldehyde dehydrogenase polymorphism is not associated with incidence of Alzheimer's disease. Int J Geriatr Psychiatry. 2005;20:1075–80.
28. Zhou S, Huriletemuer, Wang J, Zhang C, Zhao S, Wang de S, et al. Absence of association on aldehyde dehydrogenase 2 (ALDH2) polymorphism with Mongolian Alzheimer patients. Neurosci Lett. 2010;468:312–5.
29. Reichert CO, de Freitas FA, Sampaio-Silva J, Rokita-Rosa L, Barros PL, Levy D, et al. Ferroptosis mechanisms involved in neurodegenerative diseases. Int J Mol Sci. 2020;21:8765.
30. Tang D, Chen X, Kang R, Kroemer G. Ferroptosis: molecular mechanisms and health implications. Cell Res. 2021;31:107–25.
31. Stockwell BR, Friedmann Angeli JP, Bayir H, Bush AI, Conrad M, Dixon SJ, et al. Ferroptosis: a regulated cell death nexus linking metabolism, redox biology, and disease. Cell. 2017;171:273–85.
32. Yin Z, Ding G, Chen X, Qin X, Xu H, Zeng B, et al. Beclin1 haploinsufficiency rescues low ambient temperature-induced cardiac remodeling and contractile dysfunction through inhibition of ferroptosis and mitochondrial injury. Metabolism. 2020;113:154397.
33. Ren J, Zhang Y. Targeting autophagy in aging and aging-related cardiovascular diseases. Trends Pharmacol Sci. 2018;39:1064–76.
34. Gonciarz RL, Collisson EA, Renslo AR. Ferrous iron-dependent pharmacology. Trends Pharmacol Sci. 2021;42:7–18.
35. Pang J, Peng H, Wang S, Xu X, Xu F, Wang Q, et al. Mitochondrial ALDH2 protects against lipopolysaccharide-induced myocardial contractile dysfunction by suppression of ER stress and autophagy. Biochim Biophys Acta Mol Basis Dis. 2019;1865:1627–41.
36. Wang S, Wang C, Turdi S, Richmond KL, Zhang Y, Ren J. ALDH2 protects against high fat diet-induced obesity cardiomyopathy and defective autophagy: role of CaM kinase II, histone H3K9 methyltransferase SUV39H, Sirt1, and PGC-1alpha deacetylation. Int J Obes (Lond). 2018;42:1073–87.
37. Turdi S, Han X, Huff AF, Roe ND, Hu N, Gao F, et al. Cardiac-specific overexpression of catalase attenuates lipopolysaccharide-induced myocardial contractile dysfunction: role of autophagy. Free Radic Biol Med. 2012;53:1327–38.
38. Doser TA, Turdi S, Thomas DP, Epstein PN, Li SY, Ren J. Transgenic overexpression of aldehyde dehydrogenase-2 rescues chronic alcohol intake-induced myocardial hypertrophy and contractile dysfunction. Circulation. 2009;119:1941–9.
39. Zhang B, He P, Lu Y, Bian X, Yang X, Fu X, et al. HSF1 relieves amyloid-beta-induced cardiomyocytes apoptosis. Cell Biochem Biophys. 2015;72:579–87.
40. Sankpal UT, Ingersoll SB, Ahmad S, Holloway RW, Bhat VB, Simecka JW, et al. Association of Sp1 and survivin in epithelial ovarian cancer: Sp1 inhibitor and cisplatin, a novel combination for inhibiting epithelial ovarian cancer cell proliferation. Tumour Biol. 2016;37:14259–69.
41. Yamamoto T, Endo J, Kataoka M, Matsuhashi T, Katsumata Y, Shirakawa K, et al. Palmitate induces cardiomyocyte death via inositol requiring enzyme-1 (IRE1)-mediated signaling independent of X-box binding protein 1 (XBP1). Biochem Biophys Res Commun. 2020;526:122–7.
42. Yuan H, Li X, Zhang X, Kang R, Tang D. Identification of ACSL4 as a biomarker and contributor of ferroptosis. Biochem Biophys Res Commun. 2016;478:1338–43.

43. Nagahora N, Yamada H, Kikuchi S, Hakozaki M, Yano A. Nrf2 activation by 5-lipoxygenase metabolites in human umbilical vascular endothelial cells. Nutrients. 2017;9:1001.
44. Turdi S, Hu N, Ren J. Tauroursodeoxycholic acid mitigates high fat diet-induced cardiomyocyte contractile and intracellular Ca^{2+} anomalies. PLoS One. 2013;8: e63615.
45. Li Q, Wu S, Li SY, Lopez FL, Du M, Kajstura J, et al. Cardiac-specific overexpression of insulin-like growth factor 1 attenuates aging-associated cardiac diastolic contractile dysfunction and protein damage. Am J Physiol Heart Circ Physiol. 2007;292:H1398–403.
46. Peng H, Qin X, Chen S, Ceylan AF, Dong M, Lin Z, et al. Parkin deficiency accentuates chronic alcohol intake-induced tissue injury and autophagy defects in brain, liver and skeletal muscle. Acta Biochim Biophys Sin (Shanghai). 2020;52:665–74.
47. Privratsky JR, Wold LE, Sowers JR, Quinn MT, Ren J. AT1 blockade prevents glucose-induced cardiac dysfunction in ventricular myocytes: role of the AT1 receptor and NADPH oxidase. Hypertension. 2003;42:206–12.
48. Zhang Y, Xia Z, La Cour KH, Ren J. Activation of Akt rescues endoplasmic reticulum stress-impaired murine cardiac contractile function via glycogen synthase kinase-3beta-mediated suppression of mitochondrial permeation pore opening. Antioxid Redox Signal. 2011;15:2407–24.
49. Ren J, Roughead ZK, Wold LE, Norby FL, Rakoczy S, Mabey RL, et al. Increases in insulin-like growth factor-1 level and peroxidative damage after gestational ethanol exposure in rats. Pharmacol Res. 2003;47:341–7.
50. Li Y, Feng D, Wang Z, Zhao Y, Sun R, Tian D, et al. Ischemia-induced ACSL4 activation contributes to ferroptosis-mediated tissue injury in intestinal ischemia/reperfusion. Cell Death Differ. 2019;26:2284–99.
51. Wu S, Ren J. Benfotiamine alleviates diabetes-induced cerebral oxidative damage independent of advanced glycation end-product, tissue factor and TNF-alpha. Neurosci Lett. 2006;394:158–62.
52. Zhao B, Tumaneng K, Guan KL. The Hippo pathway in organ size control, tissue regeneration and stem cell self-renewal. Nat Cell Biol. 2011;13:877–83.
53. Subramanian K, Gianni D, Balla C, Assenza GE, Joshi M, Semigran MJ, et al. Cofilin-2 phosphorylation and sequestration in myocardial aggregates: novel pathogenetic mechanisms for idiopathic dilated cardiomyopathy. J Am Coll Cardiol. 2015;65:1199–214.
54. Zhao Y, Wang B, Zhang J, He D, Zhang Q, Pan C, et al. ALDH2 (Aldehyde Dehydrogenase 2) protects against hypoxia-induced pulmonary hypertension. Arterioscler Thromb Vasc Biol. 2019;39:2303–19.
55. Killion EA, Reeves AR, El Azzouny MA, Yan QW, Surujon D, Griffin JD, et al. A role for long-chain acyl-CoA synthetase-4 (ACSL4) in diet-induced phospholipid remodeling and obesity-associated adipocyte dysfunction. Mol Metab. 2018;9:43–56.
56. Yang K, Ren J, Li X, Wang Z, Xue L, Cui S, et al. Prevention of aortic dissection and aneurysm via an ALDH2-mediated switch in vascular smooth muscle cell phenotype. Eur Heart J. 2020;41:2442–53.
57. Zhang Y, Wang C, Zhou J, Sun A, Hueckstaedt LK, Ge J, et al. Complex inhibition of autophagy by mitochondrial aldehyde dehydrogenase shortens lifespan and exacerbates cardiac aging. Biochim Biophys Acta Mol Basis Dis. 2017;1863:1919–32.
58. Hu N, Ren J, Zhang Y. Mitochondrial aldehyde dehydrogenase obliterates insulin resistance-induced cardiac dysfunction through deacetylation of PGC-1alpha. Oncotarget. 2016;7:76398–414.
59. Ge W, Yuan M, Ceylan AF, Wang X, Ren J. Mitochondrial aldehyde dehydrogenase protects against doxorubicin cardiotoxicity through a transient receptor potential channel vanilloid 1-mediated mechanism. Biochim Biophys Acta. 2016;1862: 622–34.
60. Ma H, Guo R, Yu L, Zhang Y, Ren J. Aldehyde dehydrogenase 2 (ALDH2) rescues myocardial ischaemia/reperfusion injury: role of autophagy paradox and toxic aldehyde. Eur Heart J. 2011;32:1025–38.
61. Chen CH, Ferreira JC, Gross ER, Mochly-Rosen D. Targeting aldehyde dehydrogenase 2: new therapeutic opportunities. Physiol Rev. 2014;94:1–34.
62. Xu H, Zhang Y, Ren J. ALDH2 and stroke: a systematic review of the evidence. Adv Exp Med Biol. 2019;1193:195–210.